Source of Acquisition
NASA Contractor/Grantee

RM E50K10

NACA RM E50K10

RESEARCH MEMORANDUM

EXPERIMENTAL INVESTIGATION OF EFFECTS OF DESIGN CHANGES ON PERFORMANCE OF LARGE-CAPACITY CENTRIFUGAL COMPRESSORS

By Joseph R. Withee, Jr., Karl Kovach
and Ambrose Ginsburg

Lewis Flight Propulsion Laboratory
Cleveland, Ohio

NATIONAL ADVISORY COMMITTEE
FOR AERONAUTICS
WASHINGTON

March 2, 1951
Declassified December 11, 1953

NATIONAL ADVISORY COMMITTEE FOR AERONAUTICS

RESEARCH MEMORANDUM

EXPERIMENTAL INVESTIGATION OF EFFECTS OF DESIGN CHANGES ON PERFORMANCE OF LARGE-CAPACITY CENTRIFUGAL COMPRESSORS

By Joseph R. Withee, Jr., Karl Kovach, and Ambrose Ginsburg

SUMMARY

An investigation was conducted to determine the effects of several design changes on the performance of large-capacity, double-entry, centrifugal compressors. Four modifications of a turbojet-engine compressor were operated over a range of equivalent impeller tip speeds from 786 to 1545 feet per second and the compressor over-all and component performances were determined. The over-all length and diameter of the compressor assembly were constant.

Design changes that resulted in major improvements in performance were the use of a fully machined, parabolic-blade inducer, increased impeller inlet-to-outlet tip radius ratio, and a fully machined diffuser. The net gains in compressor performance at design speed were 10.3 percent in pressure ratio, 0.044 in adiabatic efficiency, and 35 percent in weight flow.

INTRODUCTION

Previous experimental investigations have determined the effects of several design variables on the performance of small-scale, centrifugal compressors and their components (references 1 to 3). Theoretical analyses also have indicated some effects of design changes on centrifugal compressors (references 4 to 6). The present investigation was conducted to determine experimentally the effects of design changes on the performance of a large-capacity centrifugal compressor from a commercial turbojet engine. The effects on compressor over-all and component performances were determined.

Design changes in the impeller included variations in the number of blades, the inlet-to-outlet tip radius ratio, and modifications to the inducer. In the diffuser, the performance effects of changes in the turning elbow, minimum throat area, and degree of finish on the wetted surfaces were investigated. This investigation consisted in operating four modifications of a large-capacity, double-entry, turbojet-engine compressor over a range of equivalent impeller tip speeds from 786 to 1545 feet per second and determining the compressor over-all and component performances. The over-all length and diameter of the compressor assembly were not changed.

This investigation was conducted at the NACA Lewis laboratory.

SYMBOLS

The following symbols are used in this report:

f_s	slip factor, ratio of tangential velocity at impeller tip to tip speed
M	Mach number
N	impeller speed, (rpm)
P	total (stagnation) pressure, (in. Hg abs.)
p	static pressure, (in. Hg abs.)
Q	volume flow, (cu ft/sec)
S	entropy
T	total (stagnation) temperature, ($^{\circ}$R)
U	impeller tip speed, (ft/sec)
V	velocity, (ft/sec)
W	weight flow, (lb/sec)
α	angle of attack, (deg)
η	diffuser efficiency
η_{ad}	adiabatic temperature-rise efficiency
δ	ratio of total (stagnation) pressure at inlet to NACA standard sea-level pressure

γ ratio of specific heats

ρ density, (slugs/cu ft)

θ ratio of total (stagnation) temperature at inlet to NACA standard sea-level temperature

Subscripts:

1 compressor inlet

2 impeller outlet

3 compressor discharge

t theoretical

APPARATUS

Four modifications of a large-capacity compressor for a commercial turbojet engine were investigated. Each compressor assembly consisted of a double-entry centrifugal impeller with an inducer section, a vaned diffuser, and a compressor casing. For each configuration the impeller tip diameter was 30.00 inches and the mean diffuser discharge diameter was 42.88 inches. The over-all length and diameter of the compressor assembly were constant. In this report the compressor models are designated by A, B, C, and D. Pertinent design data on each model are presented in table I.

The compressor assembly was mounted inside an air-tight steel tank 6 feet in diameter and approximately $13\frac{1}{2}$ feet in length, which served as a stagnation chamber. This chamber was connected to an atmospheric inlet through an orifice. Two sets of screens in the tank in addition to the large size of the tank insured uniform flow into the compressor. The turbine end of the compressor was bolted to a bulkhead plate, which was in turn bolted to the rear of the stagnation chamber. A photograph of the compressor installation is shown in figure 1. The compressor was driven by a 9000-horsepower variable-speed electric motor through a geared speed increaser.

Air was discharged from the 14 diffuser passages through 14 transition ducts into 14 discharge ducts that contained the compressor-outlet instrumentation. The air was then discharged into a central collecting chamber connected to the laboratory exhaust facilities. The inlet ducting, stagnation chamber, and discharge ducting were insulated to minimize heat transfer between the working fluid and the room air.

INSTRUMENTATION

The compressors were extensively instrumented along an air flow path so that the over-all and component performances could be determined. The stagnation state of the inlet air was based on the readings of six thermocouples and six total-pressure probes located at the root-mean-square radii of three equal annular areas in the stagnation chamber. Two static-pressure taps on opposite sides of the stagnation chamber determined the static pressure. The state of the discharge air was based on the readings of two total-pressure probes, two static-pressure taps, and one thermocouple probe located in each of the 14 discharge ducts as shown in figure 2.

Static-pressure taps were located along the front and rear impeller casings and on all four walls of one of the vaned diffuser passages to give complete coverage of an air flow path through the compressor. The number of taps varied among the compressors but was always between 90 and 100.

A spherical-type, three-dimensional survey probe was used to determine the static and total pressures and the three-dimensional flow angle at the inducer inlets. This probe consisted of a hemisphere containing five pressure taps and was mounted on a steel shaft (fig. 3). Surveys were made at both the front and rear inducer inlets for a compressor very similar to D and good agreement was found to exist between the flow conditions at the front and rear inducer inlets. Surveys were therefore made at only the front inducer inlet for compressors A, B, and D.

Total-pressure rakes were installed downstream of the diffuser turning elbow on compressor A, and upstream and downstream of the diffuser turning elbow on compressor D to determine the pressure loss through the turning vanes. Each rake consisted of 15 total-pressure probes spaced equidistant from each other to give complete coverage of the passage.

Weight-flow measurements were made with either a submerged adjustable orifice or a submerged flat-plate orifice, depending on the magnitude of the flow.

The speed of the compressor was measured with an electric chronometric tachometer.

The precision of the measurements is estimated to be within the following limits:

Temperature, °F	±0.5
Pressure, inches mercury absolute	±0.04
Air weight flow, percent	±1.0
Impeller speed, percent	±0.05

On the basis of the above limits, reproducibility of data for the condition of peak pressure ratio and design speed was within the following limits:

Compressor adiabatic temperature-rise efficiency	±0.006
Total-pressure ratio, percent	±0.3

PROCEDURE

All runs were made at ambient inlet temperatures that varied from 60° to 90° F. The runs to determine the performance characteristics of the four compressors were made at an inlet pressure of 14.0 inches of mercury absolute because of the power limitations of the drive motor. The equivalent speeds at which the four compressors were operated are given in the following table:

Equivalent impeller speed, $N/\sqrt{\theta}$ (rpm)				Equivalent tip speed, $U/\sqrt{\theta}$ (ft/sec)
A	B	C	D	
6000	6000	6000		786
			6100	799
7000	7000	7000	7000	916
			8000	1047
8500	8500	8500		1113
9000	9000	9000	9000	1178
10,000	10,000	10,000	10,000	1309
11,000	11,000	11,000	11,000	1440
[a]11,500				1505
	[a]11,750	[a]11,750		1538
			[a]11,800	1545

[a]Design speed.

Elbow surveys on compressors A and D were made at 7000 and 10,000 rpm and design speed at inlet pressures of 5.0 and 14.0 inches of mercury absolute. Inducer inlet surveys were made at design speed and peak pressure ratio.

RATING METHODS

Compressor

The equivalent weight flow $\frac{W\sqrt{\theta}}{\delta}$ and the equivalent speed $N/\sqrt{\theta}$ were computed according to the method of reference 7. Computations of adiabatic temperature-rise efficiency η_{ad} were made in accordance with reference 8.

Impeller

The impeller performance computations were based on the assumptions that: (1) The total temperature, which represents the energy input of the rotor, remains constant from the impeller exit to the measuring station in the discharge ducts; (2) the tangential velocity at the inducer inlet is zero; and (3) the velocity is constant across the diffuser passage at the impeller tip. The impeller total-pressure ratio was computed using these assumptions and the method of reference 9. It was impractical to compute the front and rear impeller pressure ratios individually. The impeller adiabatic temperature-rise efficiency was computed by using the impeller total-pressure ratio, the compressor temperature rise, and the method of reference 8.

Diffuser

The vaneless and vaned portions of the diffuser plus the turning elbows are rated together as a complete diffuser. The diffuser efficiency is defined as the ratio of the actual diffuser static-pressure rise to the theoretical diffuser static-pressure rise. This efficiency is used to compare the diffusers and is not a direct measure of the total-pressure loss through the diffuser and therefore does not directly affect the compressor efficiency. The method used to compute the diffuser efficiency is derived in the appendix.

RESULTS AND DISCUSSION

Impeller Performance

Effects of change from compressor A to compressor B. - Fully machining the inducer of compressor B allowed the leading edge of the blade to be set at the desired angle over the entire blade height. A large improvement in relative angle of attack resulted, as shown by surveys at the inducer inlet at design speed for these two compressors (fig. 4). These surveys were made only at the front inducer inlet. Good agreement, however, was found to exist between the flow conditions at the front and rear inducer inlets for a similar compressor configuration. The constant-acceleration design (parabolic blade) incorporated in the inducer of compressor B has been shown by previous investigation (references 1 and 2) to have a very beneficial effect on impeller performance. The net result of the improved angle of attack and constant-acceleration inducer is a more continuous static-pressure rise within the inducer and an increase in static pressure at the impeller exit. This fact is shown in figure 5, which presents the static-pressure ratio along the front impeller casing for compressors A and B. The leveling-off in static-pressure ratio following the rapid increase near the inlet of impeller A could be caused by separation occurring during the unloading of its inducer with resulting losses. These losses would account for the lower static-pressure ratio at the impeller exit. Another design change in the impeller was a reduction in the number of blades from 31 to 17. As will be shown later, the energy input to the air is a function of the number of blades and, therefore, this change would be expected to decrease the energy input and thus decrease the impeller total-pressure ratio. The final change was to increase the design speed by 2.2 percent, which, according to an extrapolation of the data of figure 6, would have increased the total-pressure ratio of impeller A by approximately 3.7 percent.

The net changes in impeller performance resulting from the design changes from compressor A to compressor B were an increase in the peak impeller efficiency of approximately 0.07 at all speeds (fig. 7), and an increase in the peak impeller total-pressure ratio of 13.6 percent at design speeds (fig. 6). Despite these performance increases, however, the use of a 17-blade impeller introduced intolerable vibration in the cast diffuser of compressor B.

Effects of change from compressor B to compressor C. - Increasing the number of blades from 17 to 34 by adding 17 splitter blades to impeller B increased the average slip factor f_s from 0.89 to 0.94. This increase was computed from the experimental data. The theoretical analysis of flow in this type of impeller (reference 5) indicated that the change in slip factor corresponding to this change in number of blades would be from 0.88 to 0.94. Calculations indicate that the increase in slip factor at design speed would have increased the peak total-pressure ratio by 5.5 percent if the efficiency had remained constant. The increased wetted area, however, resulted in increased surface friction for impeller C. The increased surface friction plus possible losses due to the angle of attack of the splitter blades resulted in a lower peak impeller efficiency at all speeds for impeller C (fig. 7). This decrease was 0.015 at design speed. The net result was an increase in peak total-pressure ratio of 3.4 percent at design speed (fig. 6). The increase in the number of blades did eliminate the vibration problem in the cast diffuser.

Effects of change from compressor C to compressor D. - The increase in inlet-to-outlet tip radius ratio from 0.610 to 0.649 was made to increase the weight-flow capacity of the impeller. This change was necessary because, although the diffuser is the component that limited the flow capacity of compressor C, the efficiency and pressure ratio of the impeller would be greatly decreased if only the flow capacity of the diffuser were increased, as indicated by the shape of the curves of figure 8. Although an increase in the relative Mach numbers at the tip of the inlet might be expected to increase above unity, reference 3 shows that Mach numbers in this range do not adversely affect impeller performance. Surveys at the inducer inlets showed that the increased impeller inlet-to-outlet tip radius ratio increased the relative Mach number at the inducer tip from 0.93 for impeller B to 1.03 for impeller D. Figure 9 presents the static-pressure ratio through these two impellers at design speed and indicates a more rapid static-pressure rise in the inducer of impeller D. This more rapid rise may be caused by the increase in number of inducer blades from 17 to 23. The decrease in static pressure at a distance ratio of approximately 0.5 may be caused by separation due to the more rapid change in curvature of the casing of impeller D in that region shown by figure 10. The example worked out in reference 6 to illustrate the theoretical analysis of flow presented therein was done on a similar impeller and indicated that the casing curvature can introduce adverse velocity gradients. Separation of flow due to such velocity gradients could be much more pronounced in impeller D than in impeller C because of the more rapid change in curvature noted before. Losses resulting from separation would explain the decreased static-pressure ratio at the impeller tip (fig. 9) and would reduce the impeller total-pressure ratio and efficiency. The decrease in number of impeller blades from 34 to 23 would also decrease the impeller pressure ratio for reasons previously noted. The net result of the design changes was an increase in weight-flow capacity of approximately 23 percent at design speed (fig. 8) and decreases in both peak impeller pressure ratio (fig. 6) and efficiency (fig. 7) of 12.8 percent and 0.07, respectively, at design speed.

Diffuser Performance

Effects of change from compressor A to compressor B. - The change from a constant-rate-of-diffusion turning elbow to a constant-area turning elbow and the decreased vane-leading-edge radius on compressor B resulted in an increase in peak diffuser efficiency at all speeds except design (fig. 11). The reason for the fall in efficiency at high speeds is not apparent, but it may be related to the high pressure fluctuations and cast-diffuser vibration associated with the low number of impeller blades. A possible explanation can be found in the analysis of the flow through this type of impeller according to references 4 and 5, where it was found that for ideal fluids an eddy is formed on the driving face of each impeller blade and the extent of the eddy is increased by lower impeller solidities (fewer blades) and increased wheel speeds. Although this eddy may not actually be formed for real fluids, large variations in the flow pattern leaving the impeller might be expected, which would result in adverse angles of attack on the diffuser blades.

Total-pressure rakes were installed downstream of the elbow (constant-diffusion-rate) of compressor A and both upstream and downstream of the elbow of compressor D, which had the same type of elbow (constant-area) as compressor B. The measured total-pressure loss through the constant-area elbow was compared with a computed total-pressure loss through the same elbow. The total pressure upstream was determined by adding a computed dynamic pressure to its measured static pressure. Full flow area upstream of the elbow was assumed. The total pressure downstream was that measured by the rake. This comparison is made in figure 12, where total-pressure loss is plotted against the velocity pressure at the upstream-rake position, $1\frac{1}{2}$ inches upstream of the elbow. Inasmuch as the two methods of determining pressure loss correlate, the total-pressure drop through the elbow of compressor A was computed in the same manner and is also presented in figure 12. These data indicate a total-pressure loss approximately twice as large through the constant-rate-of-diffusion elbow as through the constant-area elbow.

Effects of change from compressor B to compressor C. - No change was made in the diffuser. Figure 11, however, indicates a large gain in peak diffuser efficiency at high speeds. This increase is probably related to the improved velocity distribution resulting from the increased number of impeller blades (17 to 34) as previously noted.

Effects of change from compressor C to compressor D. - The increase in minimum diffuser throat area of 42.7 percent plus the increased capacity of the impeller (fig. 8) resulted in a 23-percent increase in maximum equivalent weight flow for compressor D at design speed (fig. 13). The closer tolerances and better finish maintained by machining all wetted surfaces increased the diffuser efficiency at all speeds, the maximum increase of 0.22 occurring at 10,000 rpm (fig. 11). At higher speeds, however, the efficiency fell off in a manner similar to diffuser B and probably for the same reasons although no vibrations were produced.

Compressor Performance

The performance maps of the four compressors investigated are presented in figure 14.

Effects of change from compressor A to compressor B. - Incorporating a fully machined, constant-acceleration inducer, decreasing the number of blades from 31 to 17, and increasing design speed by 2.2 percent resulted in an increase in peak impeller adiabatic efficiency of approximately 0.07 at all speeds and an increase in peak impeller total-pressure ratio of 13.6 percent at design speeds for impeller B. Changing from a constant-rate-of-diffusion turning elbow to a constant-area turning elbow and decreasing the vane-leading-edge radius on diffuser B caused an increase in peak diffuser efficiency at all speeds. Although the relation between diffuser efficiency and compressor efficiency is nonlinear, a higher diffuser efficiency does result in higher compressor performance. The effects of the component changes on compressor performance were an increase in peak adiabatic efficiency at all speeds amounting to 0.055 at design speeds (fig. 15), an increase in peak total-pressure ratio at all speeds amounting to 10.0 percent at design speeds (fig. 16), and an increase in maximum equivalent weight flow of 4.7 percent at design speeds (fig. 13). The increases in compressor performance are not as large as would be expected from the improvements in component performance because the peak compressor performance did not occur at the same flow points as the peak component performances. Although the change from compressor A to compressor B resulted in greatly improved performance, the use of a 17-blade impeller introduced intolerable vibration in the cast diffuser.

Effects of change from compressor B to compressor C. - Increasing the number of impeller blades from 17 to 34 increased the peak impeller total-pressure ratio 3.4 percent at design speed and decreased the peak impeller efficiency 0.015 at design speed. No design changes were made in the diffuser. The peak diffuser efficiency, however, increased markedly at high speeds. The effects of the component changes on compressor performance were an increase in peak total-pressure ratio of 2.7 percent at design speed (fig. 16), a decrease in peak compressor efficiency at all speeds except design, (reaching a maximum of 0.035 at 9000 rpm (fig. 15)), and an increase in maximum equivalent weight flow of 4.2 percent at design speed (fig. 13). In this case the decrease in compressor efficiency is approximately equal to the decrease in impeller efficiency except at design speed, which is the only speed at which a large increase in diffuser efficiency occurs. The increased number of impeller blades eliminated the vibration in the diffuser casting.

Effects of change from compressor C to compressor D. - Increasing the inlet-to-outlet tip radius ratio from 0.610 to 0.649 and decreasing the number of impeller blades from 34 to 23 decreased the peak impeller total-pressure ratio and efficiency at design speeds by 12.8 percent and 0.07, respectively, but the weight-flow capacity of the impeller was increased by approximately 23 percent. Increasing the diffuser minimum throat area by 42.7 percent and fully machining all the wetted surfaces increased the diffuser efficiency at all speeds, the maximum increase of 0.22 occurring at 10,000 rpm. The effects of the component changes on compressor performance were an increase in maximum equivalent weight flow of approximately 23 percent at design speeds (fig. 13), a decrease of 2.2 percent in peak compressor total-pressure ratio at design speeds (fig. 16), and an increase of approximately 0.015 in peak compressor efficiency at all speeds except design (fig. 15). In this case, the increased diffuser efficiency compensates for the decrease in impeller performance.

Effects of change from compressor A to compressor D. - The net results of all the design changes made during this investigation were the following improvements in compressor performance at design speeds: (1) peak compressor total-pressure ratio, 10.3 percent; (2) peak compressor adiabatic efficiency, 0.044; and (3) maximum equivalent weight flow, 35 percent.

SUMMARY OF RESULTS

An investigation of a series of modifications in a large-capacity, double-entry centrifugal compressor for a turbojet engine produced the following results:

1. Changing from a bent-bucket, circular-arc inducer to a fully machined, constant-acceleration inducer was the primary reason for an increase of 0.07 in peak impeller efficiency at all speeds and an increase of 13.6 percent in peak impeller total-pressure ratio at design speeds.

2. Increasing the inlet-to-outlet tip radius ratio from 0.610 to 0.649 with an accompanying increase in the rate of curvature of the casing was the main reason for an increase of approximately 23 percent in weight-flow capacity at design speeds. However, the impeller pressure ratio and efficiency decreased 12.8 and 0.07, respectively, at design speeds.

3. Fully machining all wetted surfaces in the vaned diffuser resulted in a maximum increase in diffuser efficiency of 0.22 at 10,000 rpm.

4. Reducing the number of impeller blades to 17 caused intolerable vibration in the cast diffuser at high speeds, which was accompanied by decreases in compressor and diffuser efficiencies.

5. Changing from a constant-rate-of-diffusion turning elbow to a constant-area turning elbow in the vaned diffuser appeared to decrease the pressure loss through the elbow by approximately one-half, thus tending to increase the compressor pressure ratio and efficiency.

6. The following improvements in compressor performance at design speed were achieved with no increase in over-all dimensions and an increase in equivalent speed of only 2.6 percent: (1) peak compressor pressure ratio, 10.3 percent; (2) peak adiabatic temperature-rise efficiency, 0.044; and (3) maximum weight flow, 35 percent.

Lewis Flight Propulsion Laboratory,
National Advisory Committee for Aeronautics,
Cleveland, Ohio.

APPENDIX - METHOD OF COMPUTING DIFFUSER EFFICIENCY

The total and static pressures involved in computing the diffuser efficiency are presented in the following sketch of a temperature-entropy diagram:

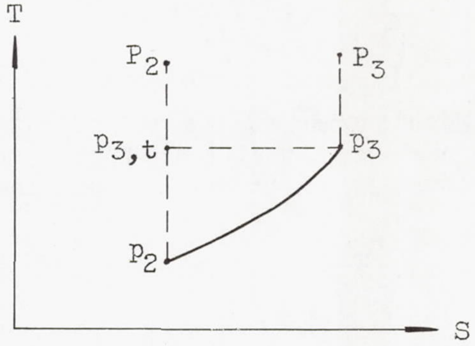

Conditions at the diffuser inlet are represented by P_2 and p_2. Theoretically, there should be no entropy change through the diffuser, and $p_{3,t}$ would lie on a constant-entropy line. Actually there is an entropy increase with a resulting total-pressure loss and, therefore, P_3 and p_3 are at different entropy levels.

By definition, the diffuser efficiency η is expressed

$$\eta = \frac{p_3 - p_2}{p_{3,t} - p_2} \tag{1}$$

Multiplying and dividing by p_2 gives

$$\eta = \frac{\frac{p_3}{p_2} - 1}{\frac{p_{3,t}}{p_2} - 1} \tag{2}$$

$p_{3,t}/p_2$ may be written

$$\frac{p_{3,t}}{p_2} = \frac{\frac{P_2}{p_2}}{\frac{P_2}{p_{3,t}}} \tag{3}$$

The relation between the total and static pressure at any point can be expressed in terms of the Mach number at that point by the following form of Bernoulli's equation:

$$\frac{P}{p} = \left(1 + \frac{\gamma-1}{2} M^2\right)^{\frac{\gamma}{\gamma-1}} \qquad (4)$$

If the theoretical Mach number at the diffuser discharge is assumed equal to the actual Mach number at that point, then from equation (4) and the temperature-entropy diagram it can be seen that

$$\frac{P_2}{p_{3,t}} = \frac{P_3}{p_3} \qquad (5)$$

By combining equations (2), (3), and (5)

$$\eta = \frac{\dfrac{p_3}{p_2} - 1}{\dfrac{P_2/p_2}{P_3/p_3} - 1} \qquad (6)$$

Because p_3, p_2, and P_3 are measured, and P_2 is computed for the impeller pressure ratio, the diffuser efficiency can be computed from equation (6).

REFERENCES

1. Ritter, William K., and Johnsen, Irving A.: Preliminary Investigation of Deep Inducers as Separate Supercharger Components. NACA ARR E5I28, 1945.

2. Ritter, William K., Ginsburg, Ambrose, and Beede, William L.: Performance Comparison of Two Deep Inducers as Separate Components and in Combination with an Impeller. NACA ARR E5J03, 1945.

3. Ginsburg, Ambrose, Ritter, William K., and Palasics, John: Effects on Performance of Changing the Division of Work between Increase of Angular Velocity and Increase of Radius of Rotation in an Impeller. NACA TN 1216, 1947.

4. Stanitz, John D.: Two-Dimensional Compressible Flow in Turbomachines with Conic Flow Surfaces. NACA Rep. 935, 1949. (Formerly NACA TN 1744.)

5. Stanitz, John D., and Ellis, Gaylord O.: Two-Dimensional Compressible Flow in Centrifugal Compressors with Straight Blades. NACA Rep. 954, 1950. (Formerly NACA TN 1932.)

6. Hamrick, Joseph T., Ginsburg, Ambrose, and Osborn, Walter M.: Method of Analysis for Compressible Flow through Mixed-Flow Centrifugal Impellers of Arbitrary Design. NACA TN 2165, 1950.

7. NACA Subcommittee on Compressors: Standard Procedures for Rating and Testing Multistage Axial-Flow Compressors. NACA TN 1138, 1946.

8. Ellerbrock, Herman H., Jr., and Goldstein, Arthur W.: Principles and Methods of Rating and Testing Centrifugal Superchargers. NACA ARR, Feb. 1942.

9. Ginsburg, Ambrose, Johnsen, Irving A., and Redlitz, Alfred C.: Determination of Centrifugal-Compressor Performance on Basis of Static-Pressure Measurements in Vaneless Diffuser. NACA TN 1880, 1949.

TABLE I - DESIGN DATA ON COMPRESSOR CONFIGURATIONS

Compressor	Design flow (lb/sec)	Inducer	Impeller	Diffuser
A	75	Bent bucket, approximately a circular arc Inlet tip diameter = 18.31 inches Blade angle at root = 81°[a] Blade angle at tip = 28°[a] Inlet eye area = 2.962 square feet Design relative Mach number at inlet tip for design flow at design speed = 0.891 Number of blades = 31 per side	31 straight radial blades Tip diameter = 30.00 inches Inlet-to-outlet tip radius ratio = 0.610 Blade depth including inducer = 5.50 inches	Cast; vane tips shaped by hand Leading-edge radius = 0.070 inch Inlet angle = 14.5° Vane tip diameter = 34.09 inches Minimum throat area = 4.79 square inches for each of 14 passages Constant-width passage approaching turning elbow, with expanding area within elbow
B	85	Separate component, fully machined, parabolic blade Inlet tip diameter = 18.31 inches Blade angle at root = 42°[a] Blade angle at tip = 30.9°[a] Inlet eye area = 2.998 square feet Depth = 2.812 inches Design relative Mach number at inlet tip for design flow at design speed = 0.910 Number of blades = 17 per side	17 straight radial blades Tip diameter = 30.00 inches Inlet-to-outlet tip radius ratio = 0.610 Blade depth not including inducer = 3.50 inches	Main part of diffuser cast; inlet tips are stainless-steel inserts with leading-edge radius of 0.015 inch Inlet angle = 15.0° Vane tip diameter = 33.78 inches Minimum throat area = 4.71 square inches for each of 14 passages Widening passage approaching turning elbow, with constant area in elbow
C	85	Same as Compressor B	17 splitter blades added to 17-blade impeller	Same as Compressor B
D	105	Separate component; fully machined, parabolic blade Inlet tip diameter = 19.48 inches Blade angle at root = 56.6°[a] Blade angle at tip = 31.7°[a] Inlet eye area = 3.523 square feet Depth = 3.500 inches Design relative Mach number at inlet tip for design flow at design speed = 0.995 Number of blades = 23 per side	23 straight radial blades Tip diameter = 30.00 inches Inlet-to-outlet tip radius ratio = 0.649 Blade depth not including inducer = 3.43 inches	Two-piece; all wetted surfaces fully machined Leading-edge radius = 0.018 inch Inlet angle = 18.3° Vane tip diameter = 34.50 inches Minimum throat area = 6.72 square inches for each of 14 passages Widening passage approaching turning elbow, with constant area in elbow

[a] Angle measured with respect to plane normal to axis of rotation.

NACA

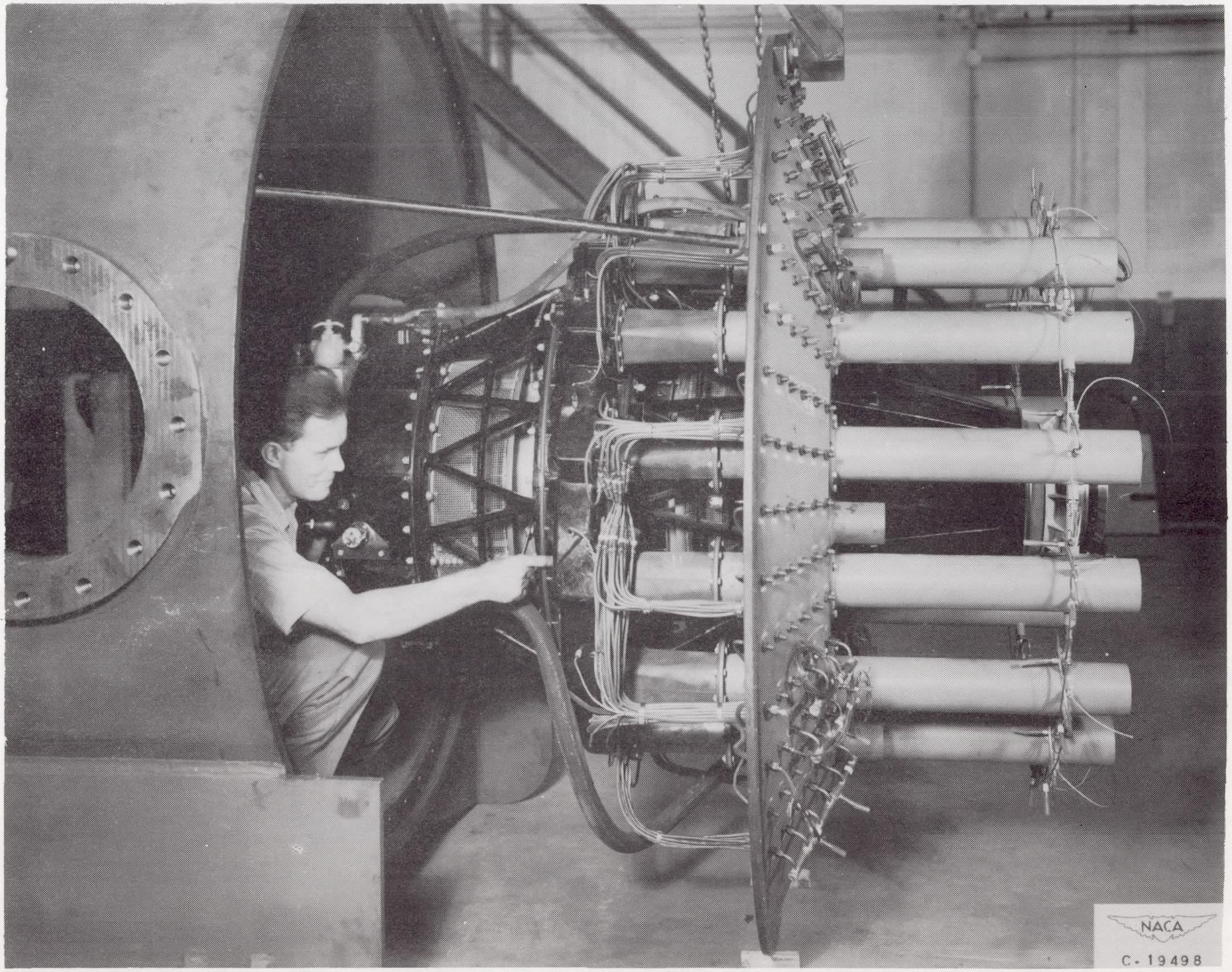
NACA
C-19498

Figure 1. - Installation of large-capacity centrifugal compressor.

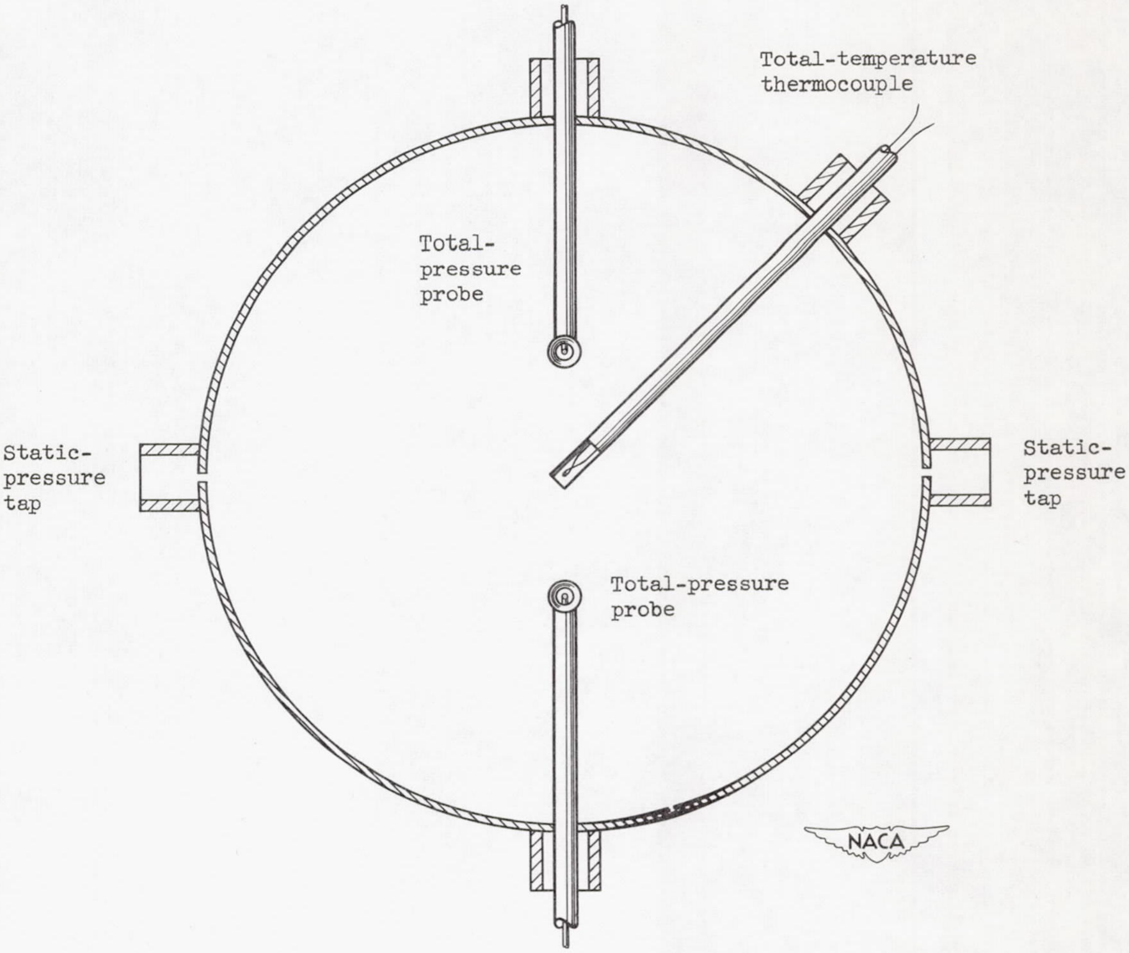
Total-temperature thermocouple
Total-pressure probe
Static-pressure tap
Static-pressure tap
Total-pressure probe

Figure 2. - Typical instrumentation of a discharge duct.

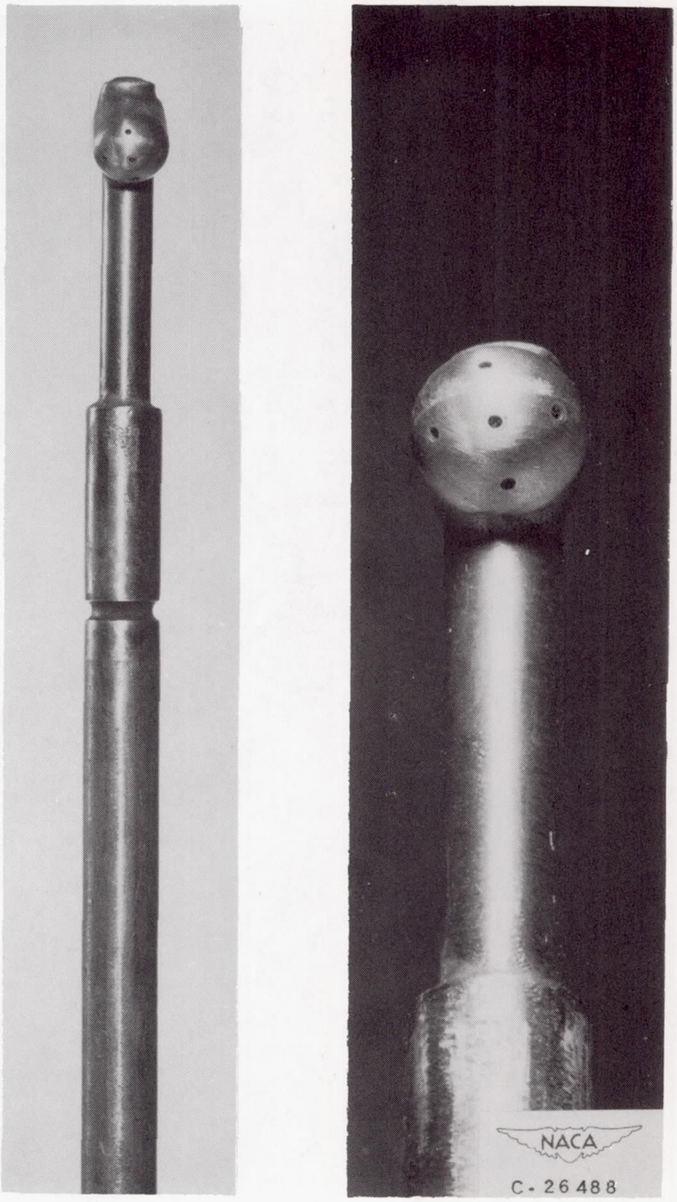
NACA
C-26488

Figure 3. - Spherical-type, three-dimensional survey probe.

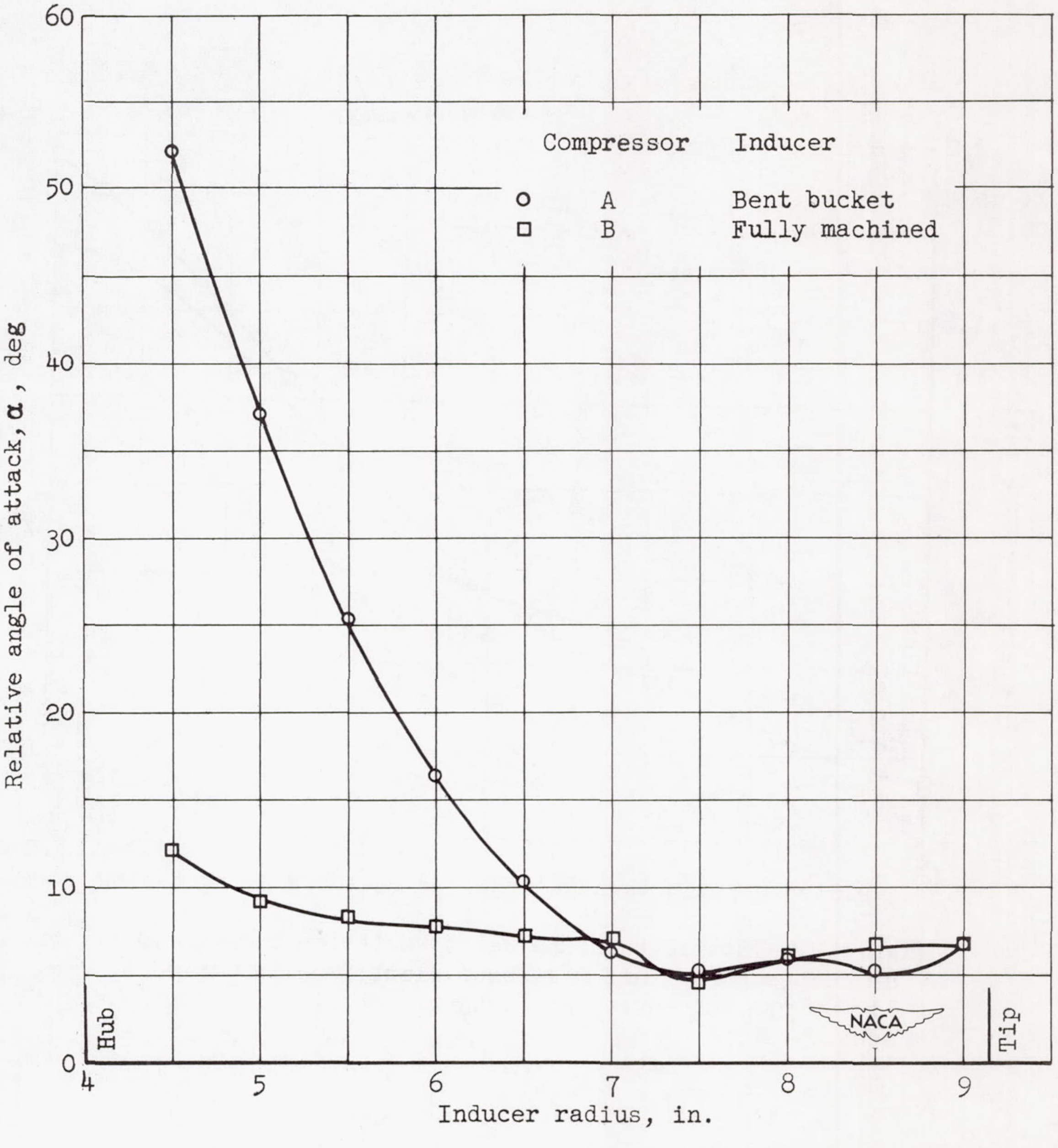

Figure 4. - Radial variation of relative angle of attack at inducer inlet at design speed for compressors A and B.

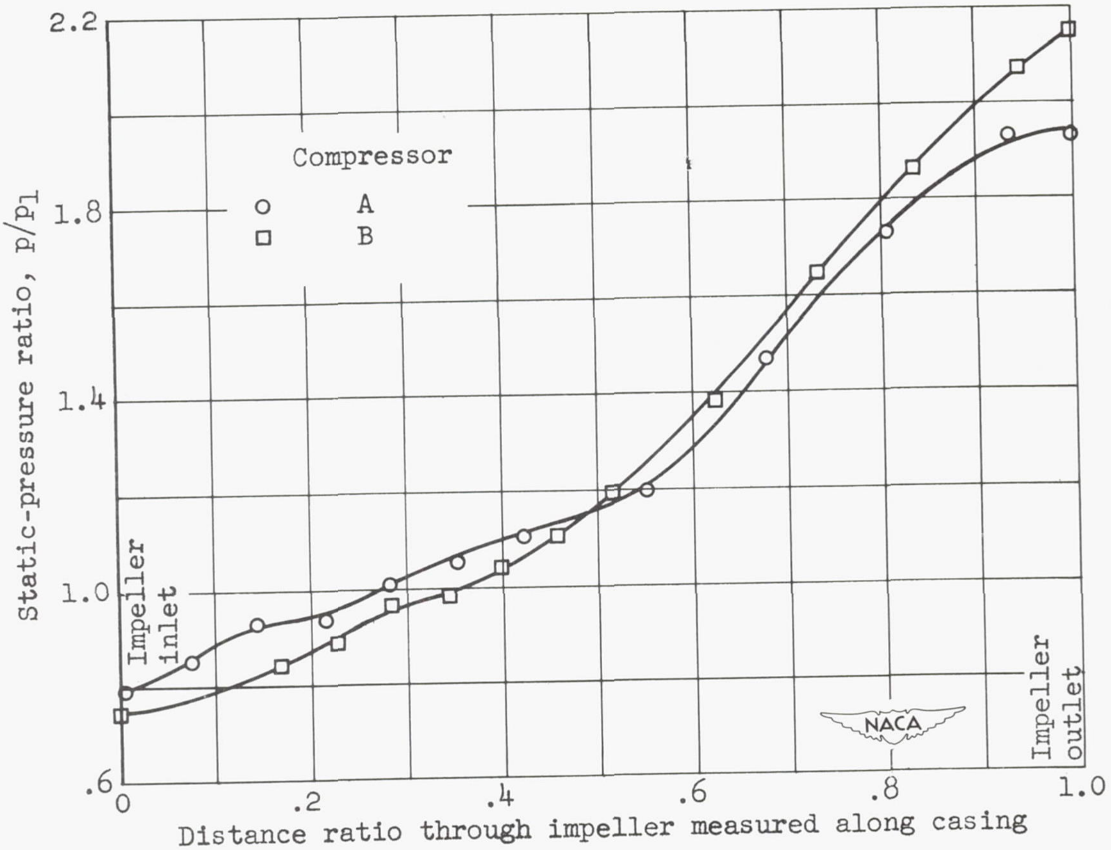

Figure 5. - Static-pressure-ratio variation through impellers of compressors A and B at equivalent impeller speed of 11,000 rpm and equivalent weight flow of 79.6 pounds per second.

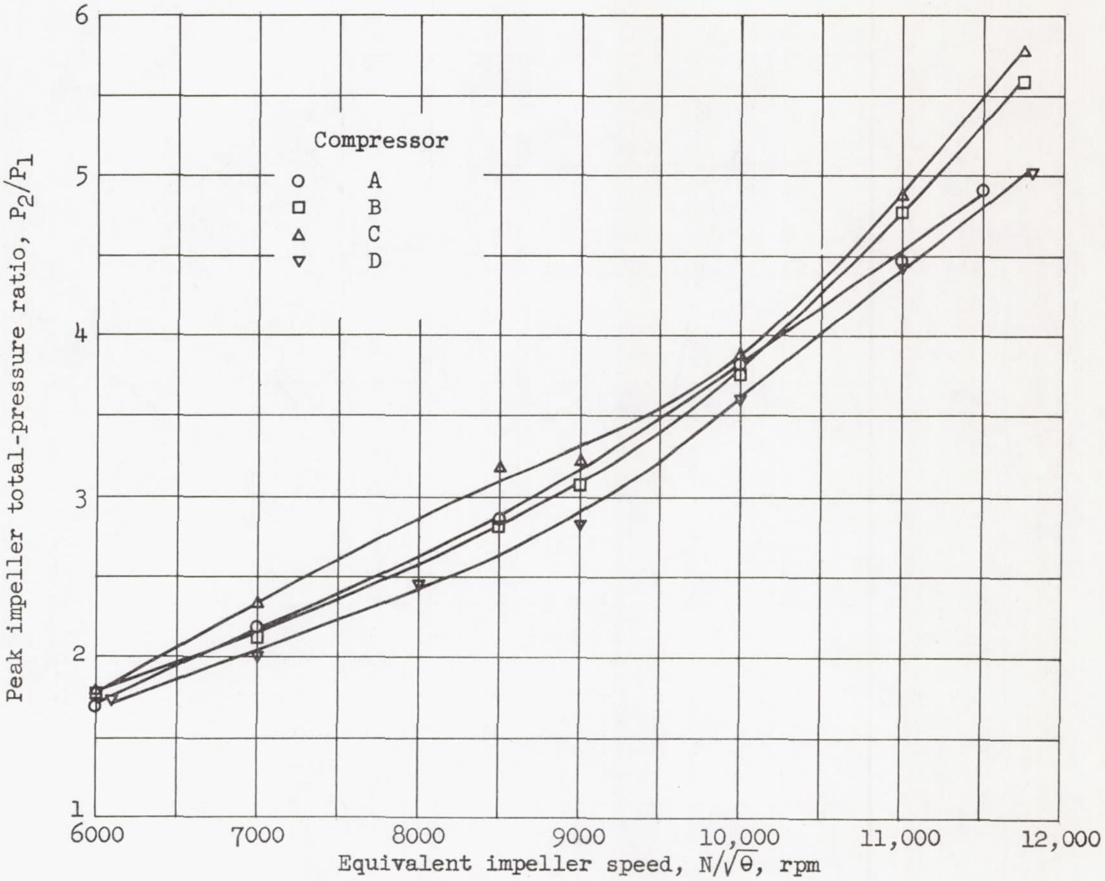

Figure 6. - Variation of peak impeller total-pressure ratio with speed for four compressors.

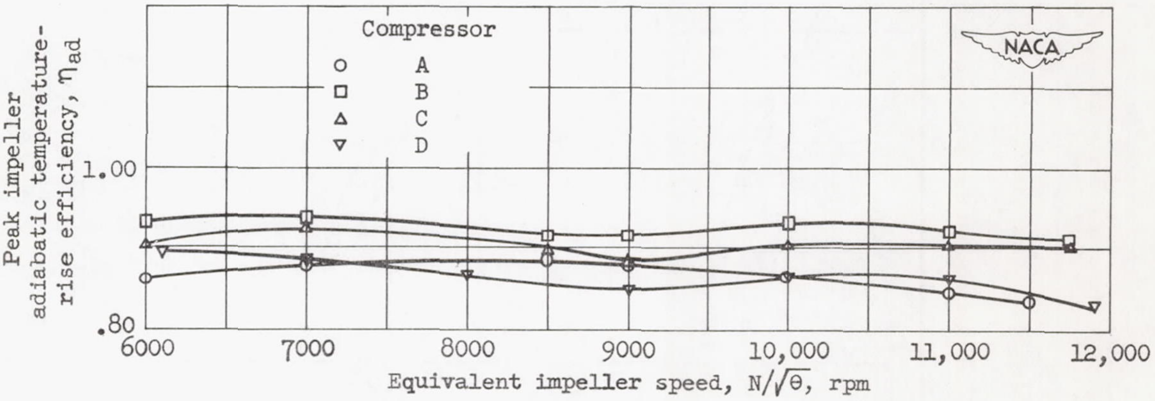

Figure 7. - Variation of peak impeller efficiency with speed for four compressors.

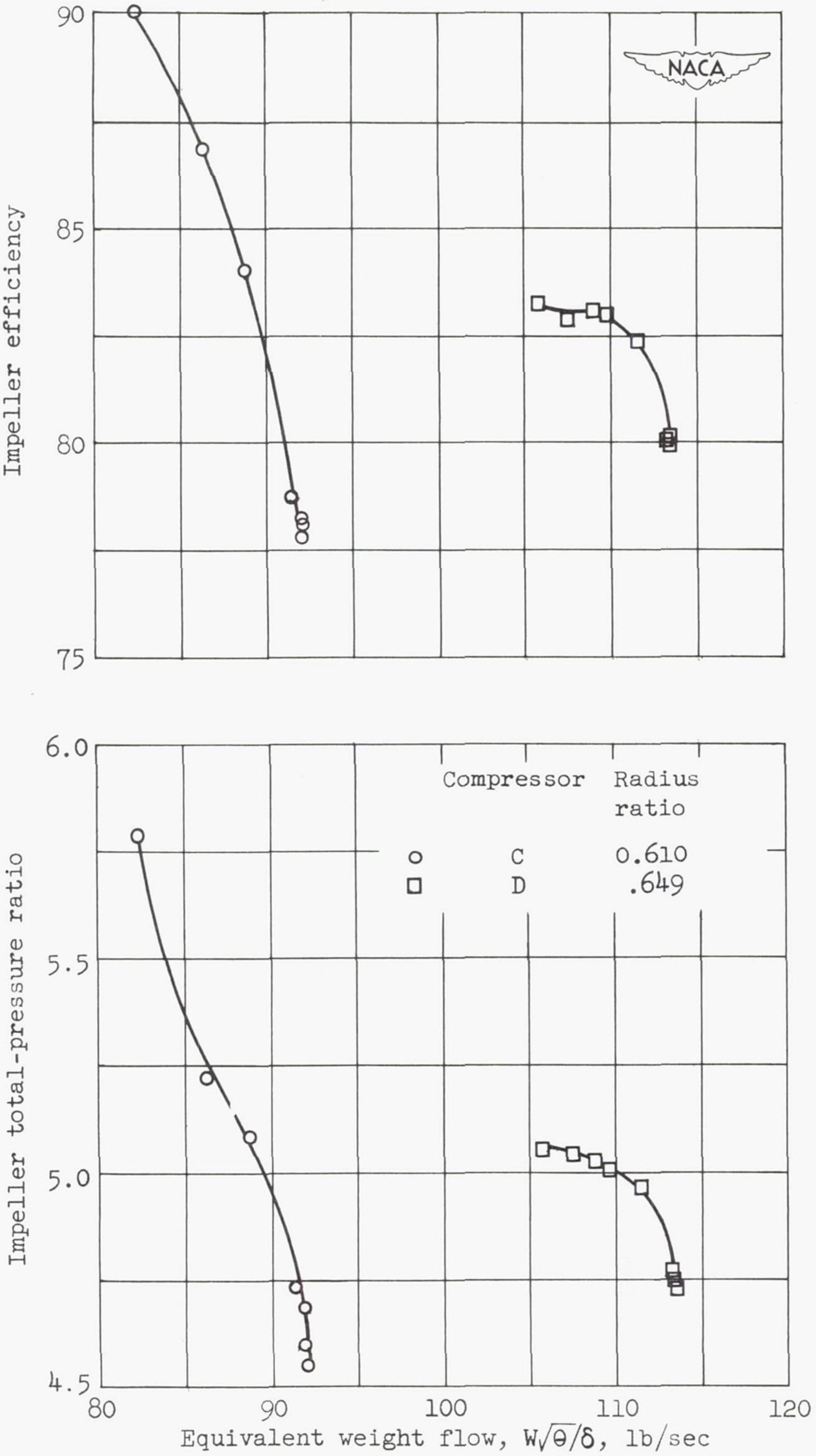

Figure 8. - Variation of impeller pressure ratio and efficiency with equivalent weight flow at design speeds for compressors C and D.

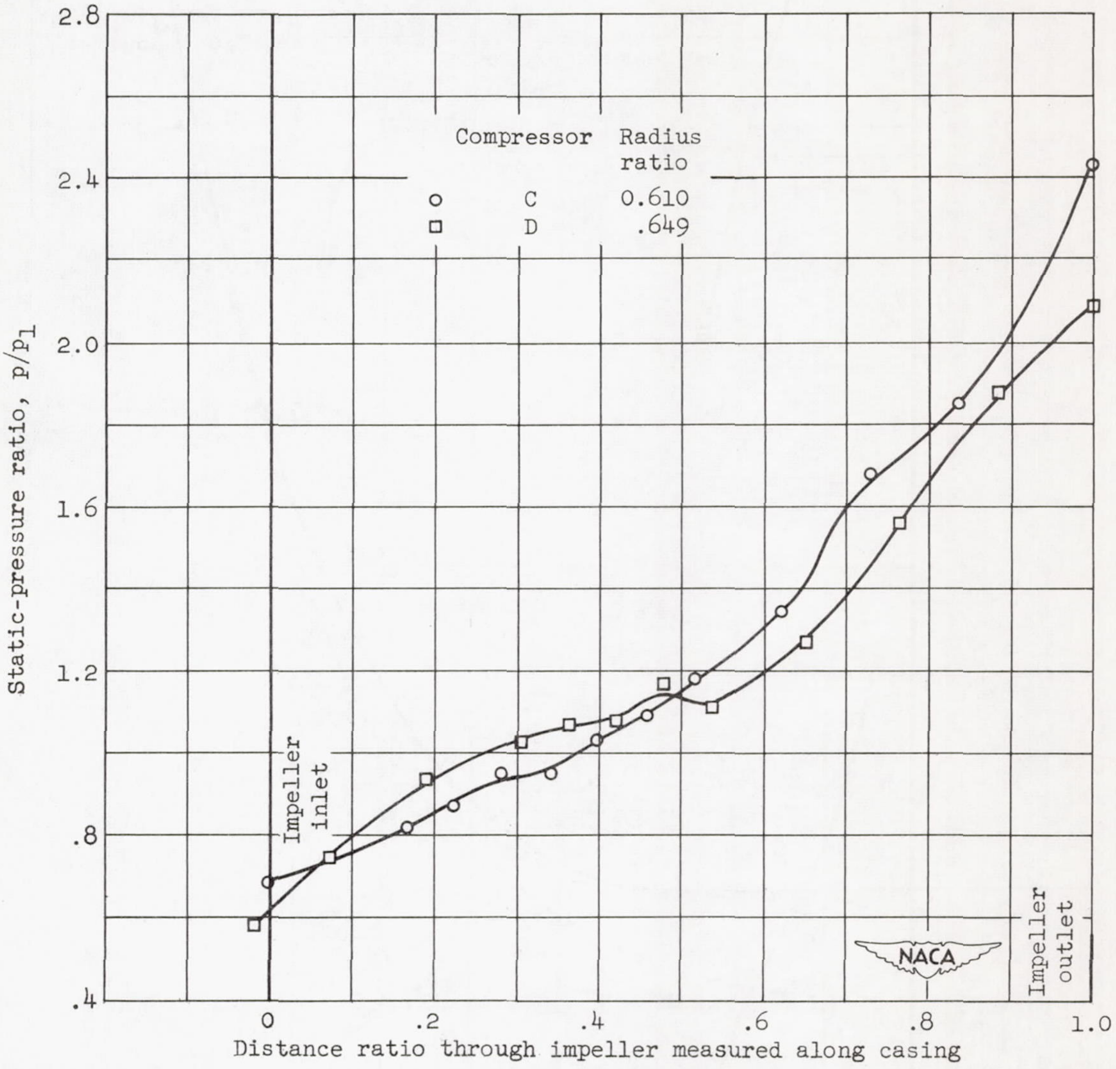

Figure 9. - Static-pressure ratio variation through impellers of compressors C and D at peak over-all efficiency and design equivalent impeller speed.

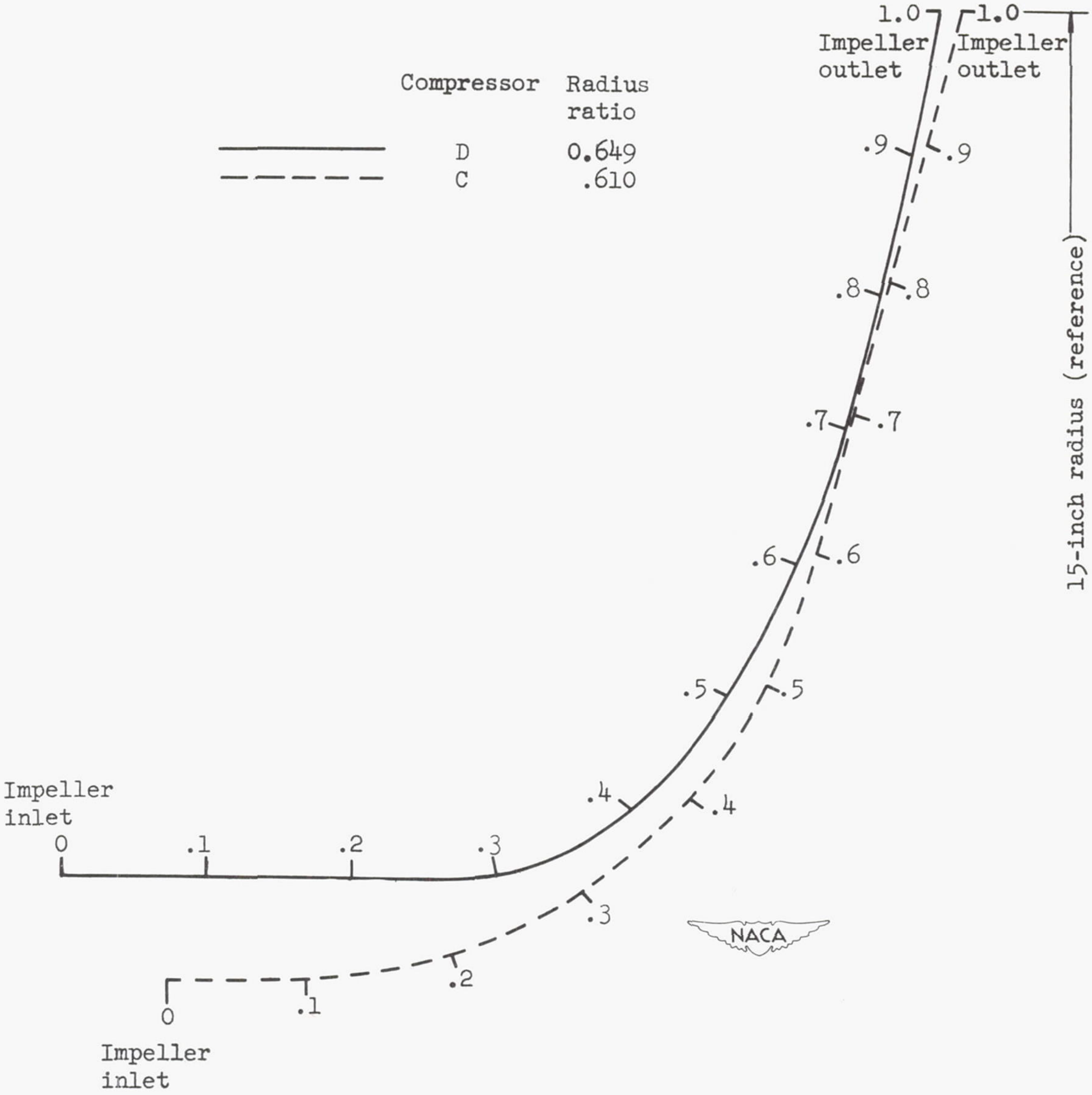
Compressor
Radius ratio
D 0.649
C .610
1.0
Impeller outlet
1.0
Impeller outlet
.9
.9
.8
.8
.7
.7
.6
.6
.5
.5
.4
.4
.3
.3
.2
.2
.1
.1
0
0
Impeller inlet
Impeller inlet
15-inch radius (reference)
NACA

Figure 10. - Distance ratios along casings of compressors C and D.

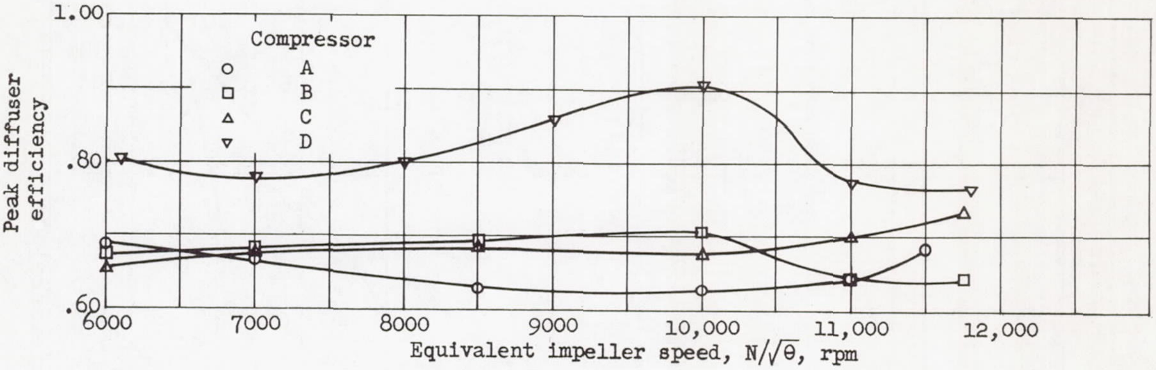

Figure 11. - Variation of peak diffuser efficiency with speed for four compressors.

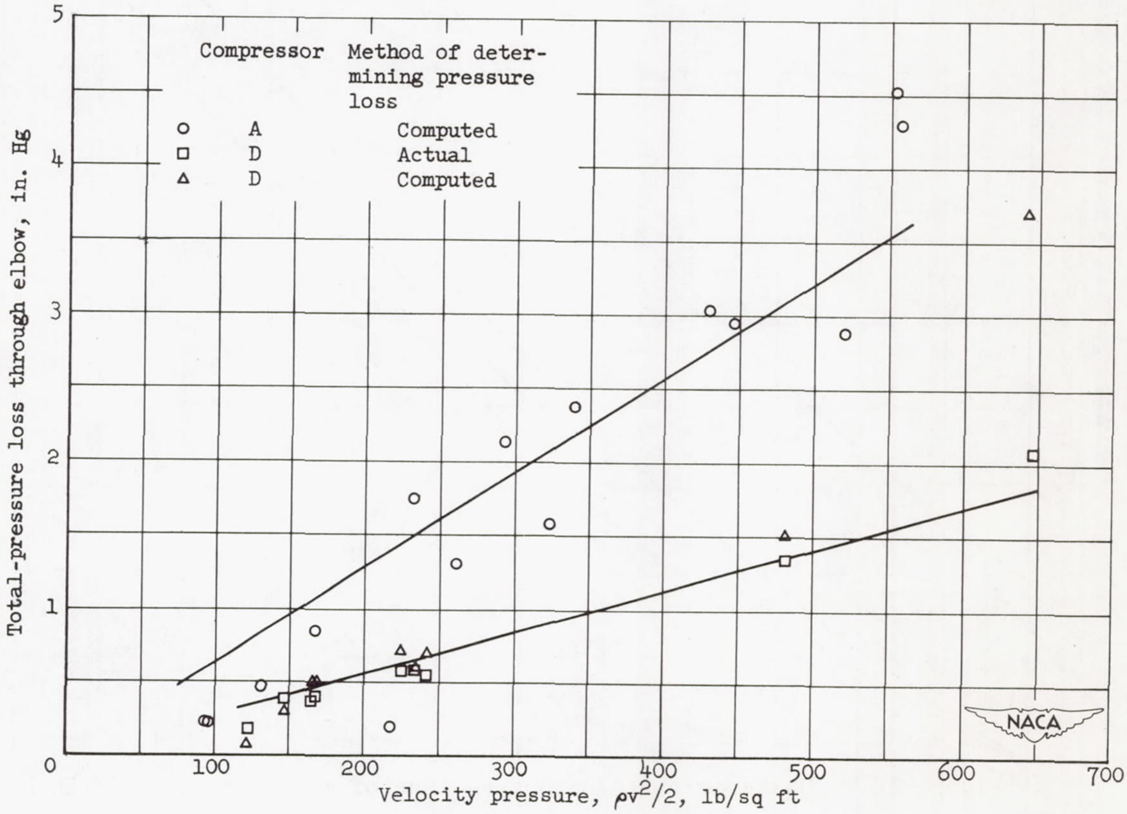

Figure 12. - Total-pressure loss through vaned turning elbows of compressors A and D.

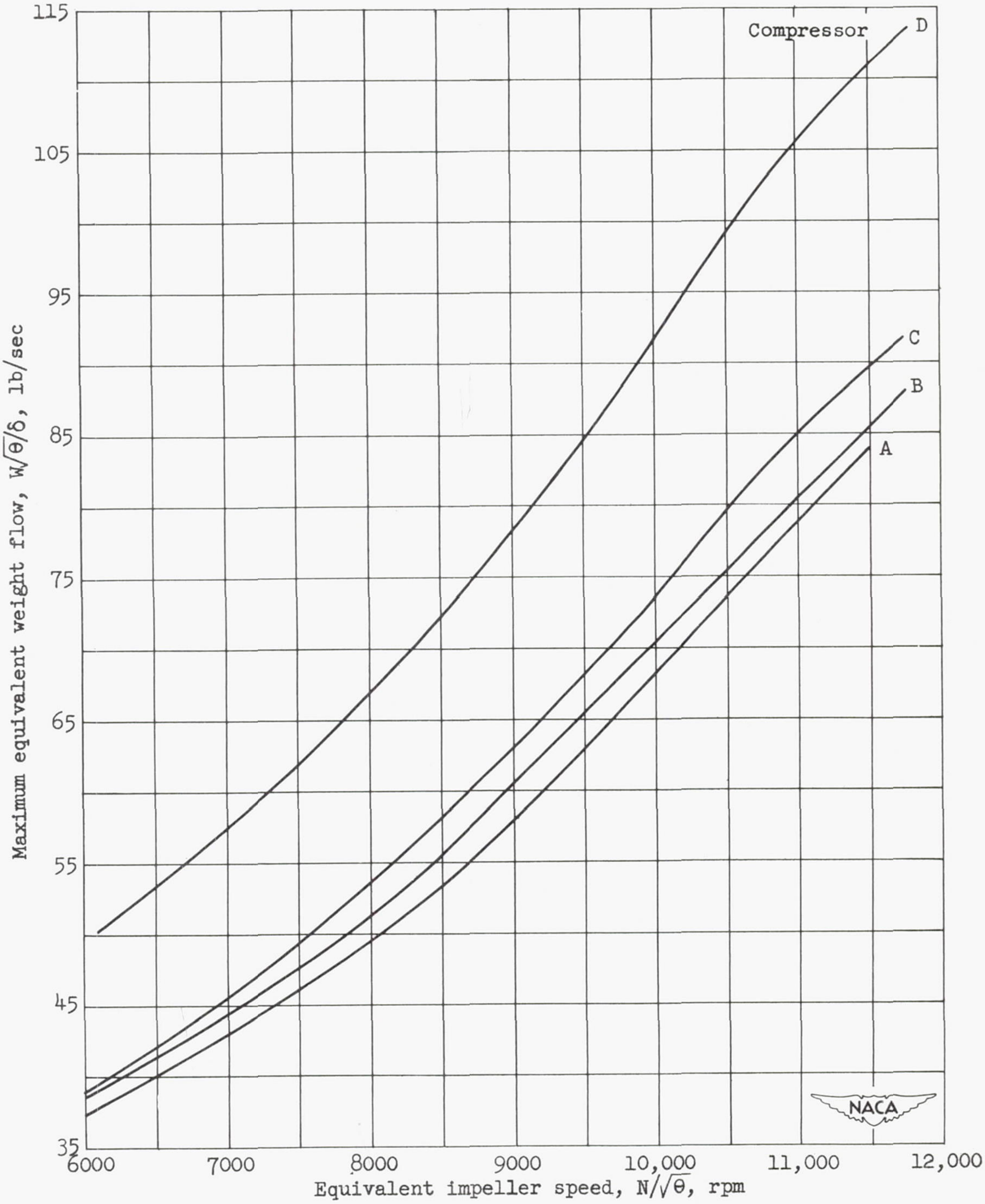

Figure 13. - Variation of maximum equivalent weight flow with speed for four compressors.

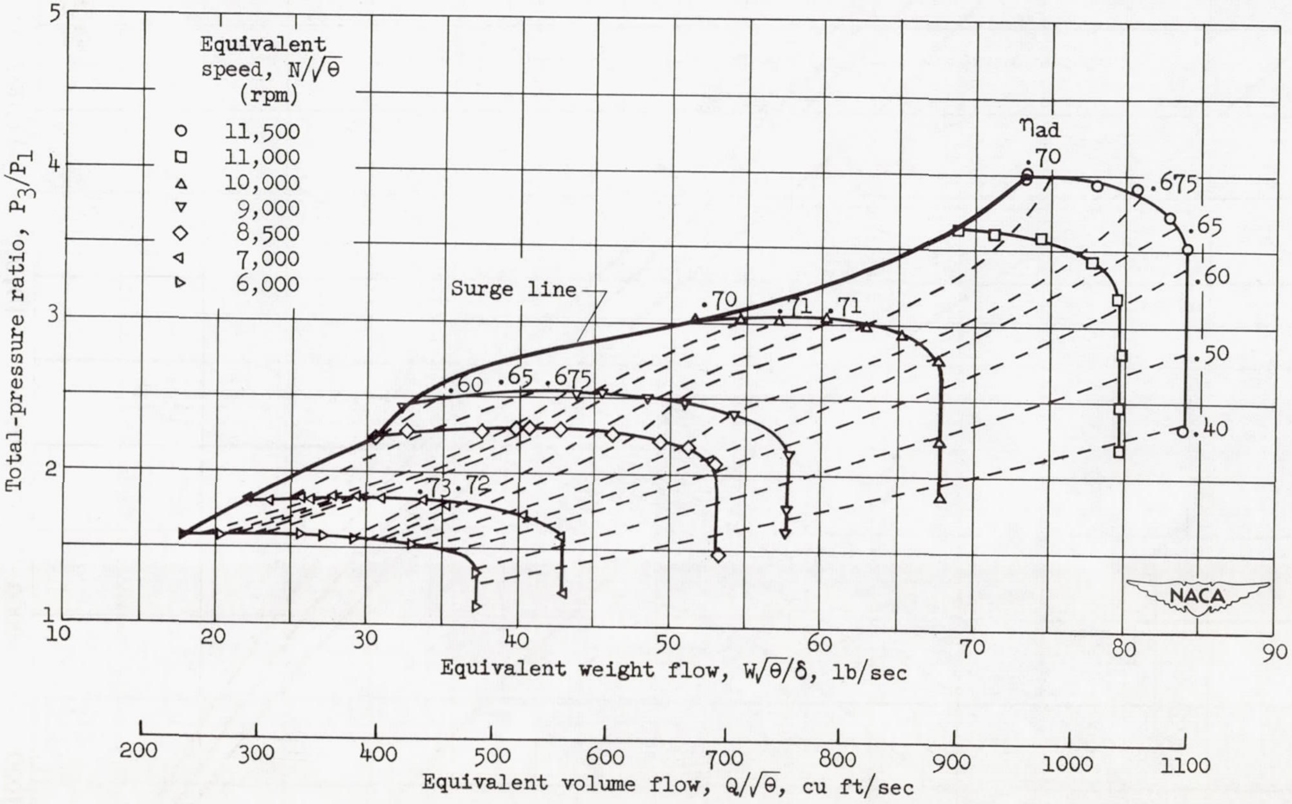

(a) Compressor A.

Figure 14. - Over-all performance of four compressor models.

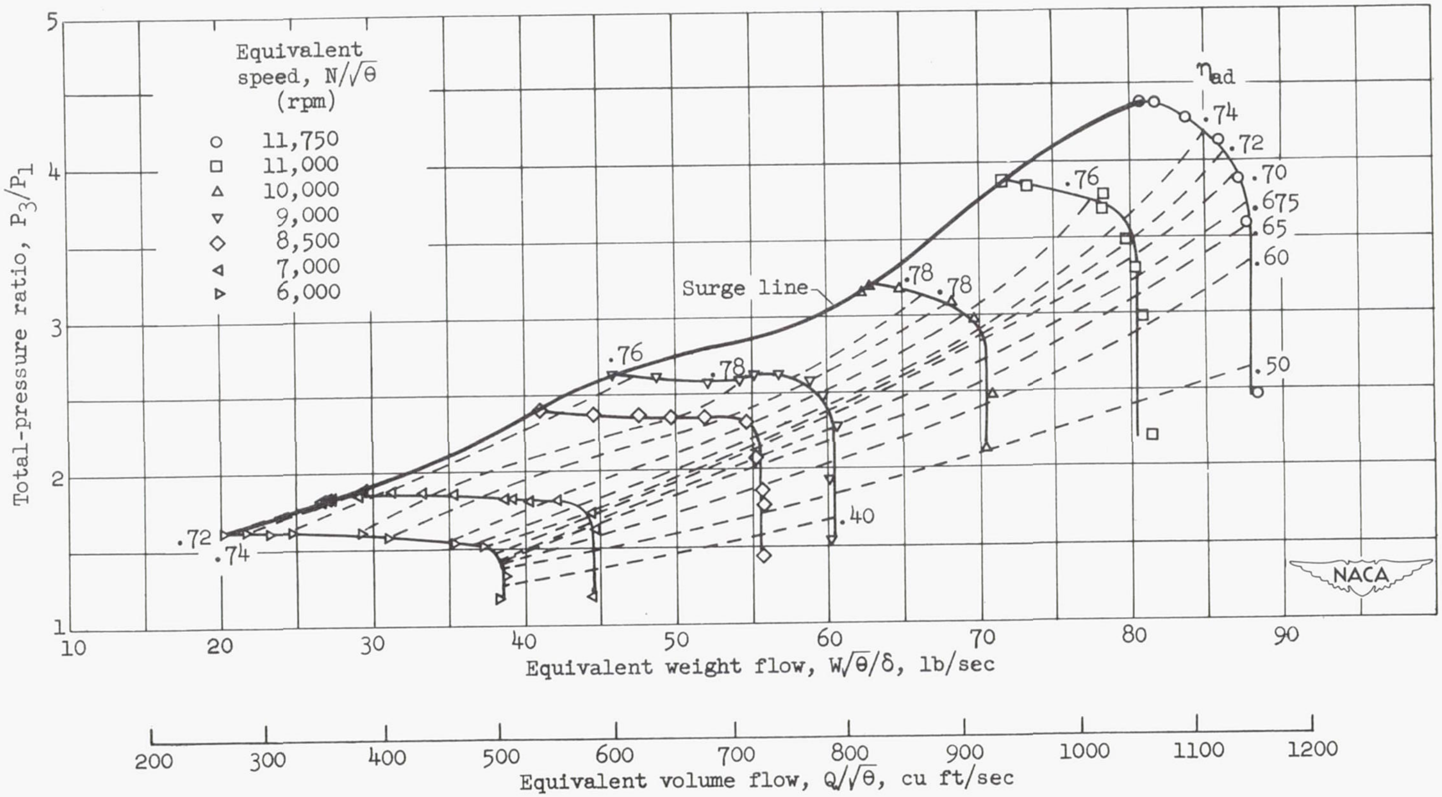

(b) Compressor B.

Figure 14. - Continued. Over-all performance of four compressor models.

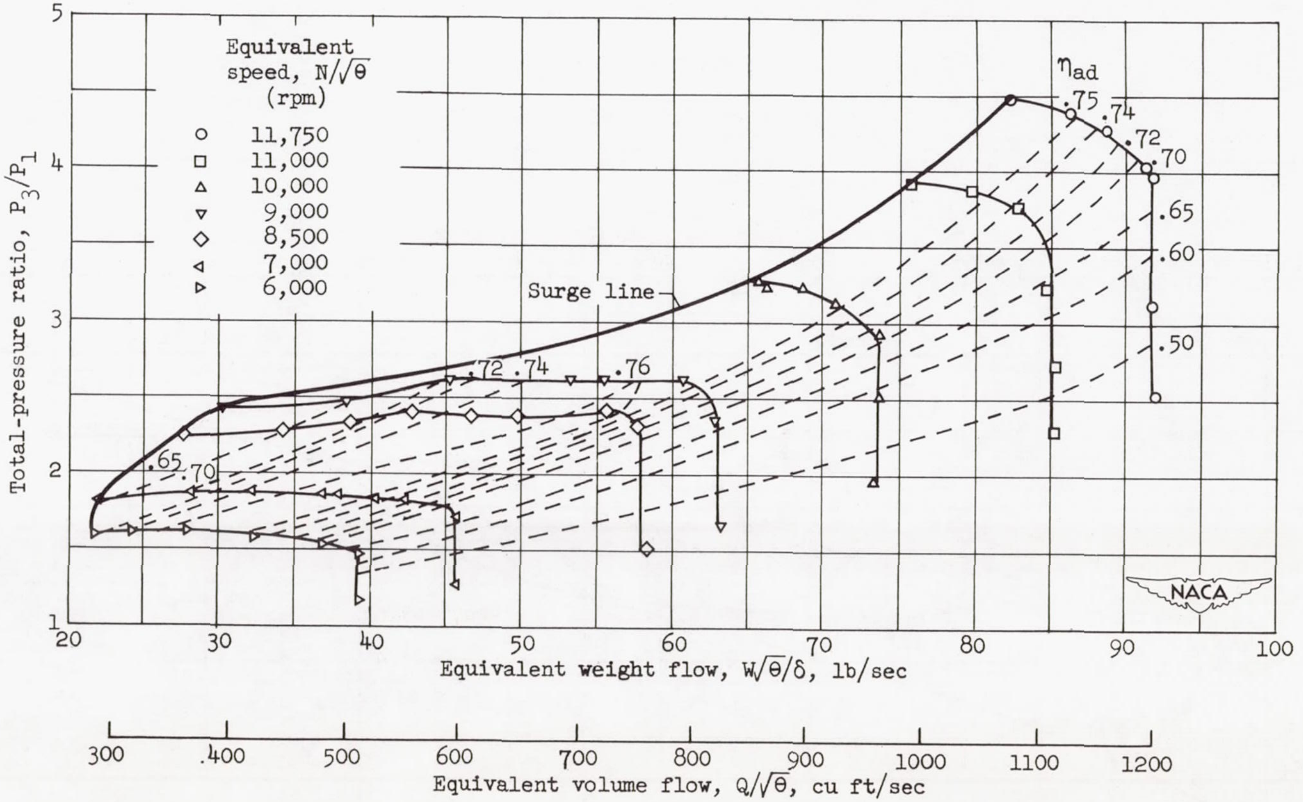

(c) Compressor C.

Figure 14. - Continued. Over-all performance of four compressor models.

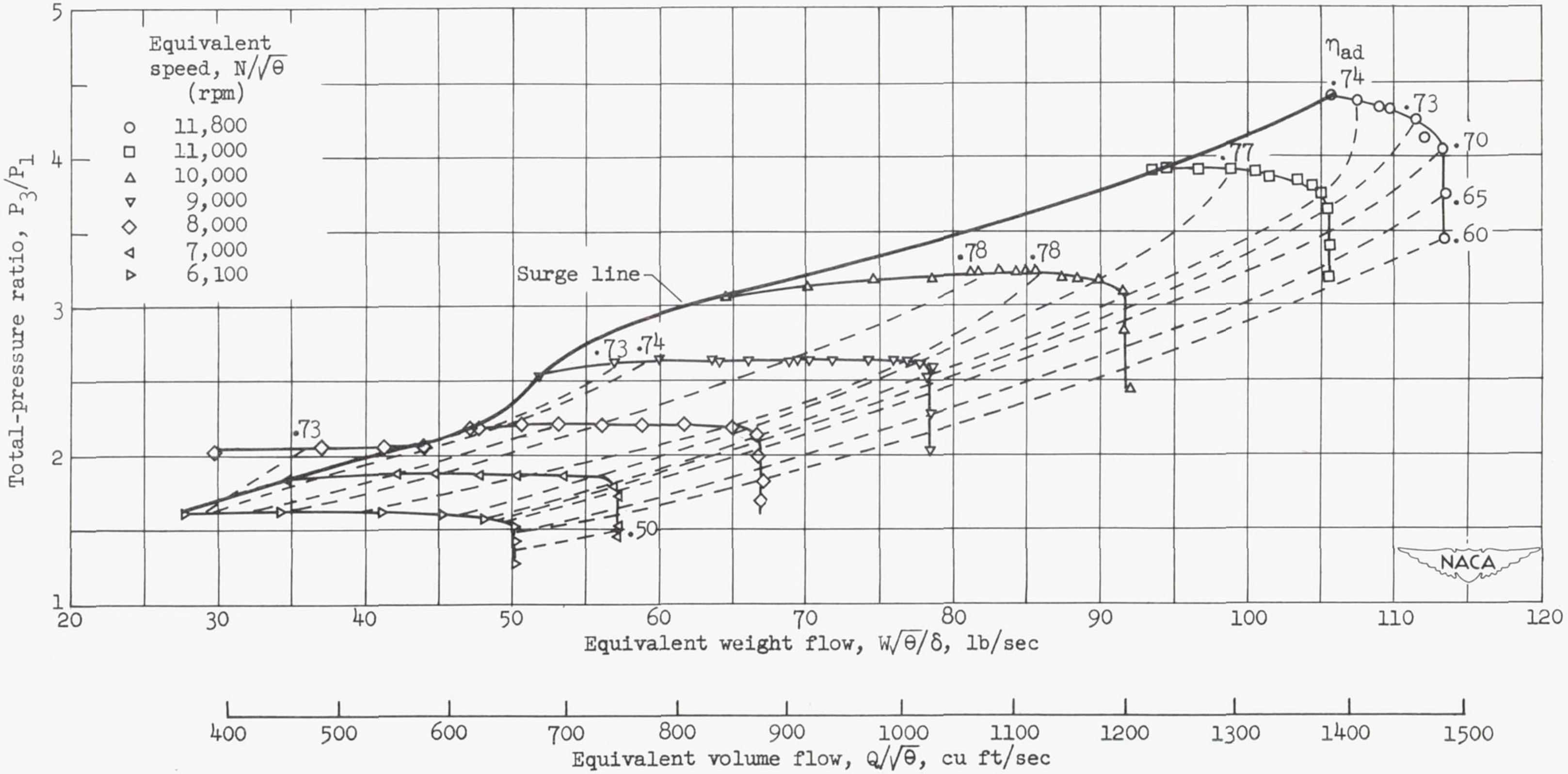

(d) Compressor D.

Figure 14. - Concluded. Over-all performance of four compressor models.

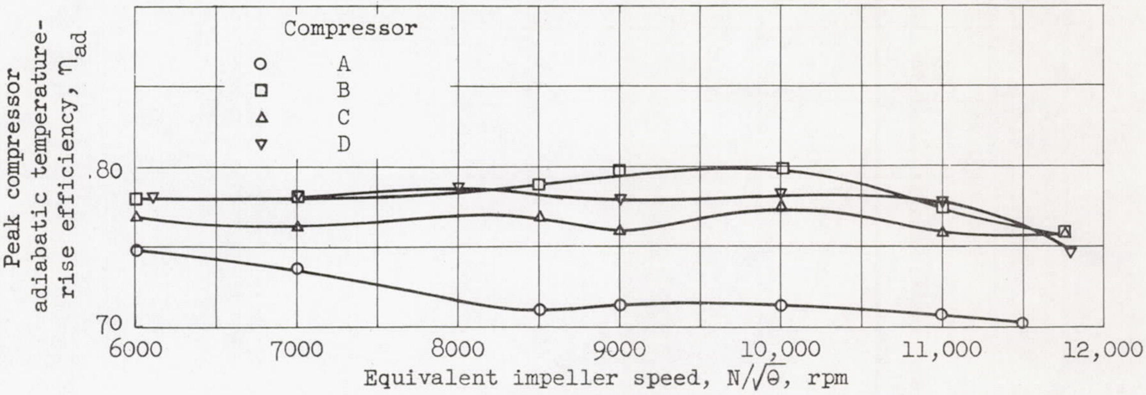

Figure 15. - Variation of peak compressor efficiency with speed for four compressors.

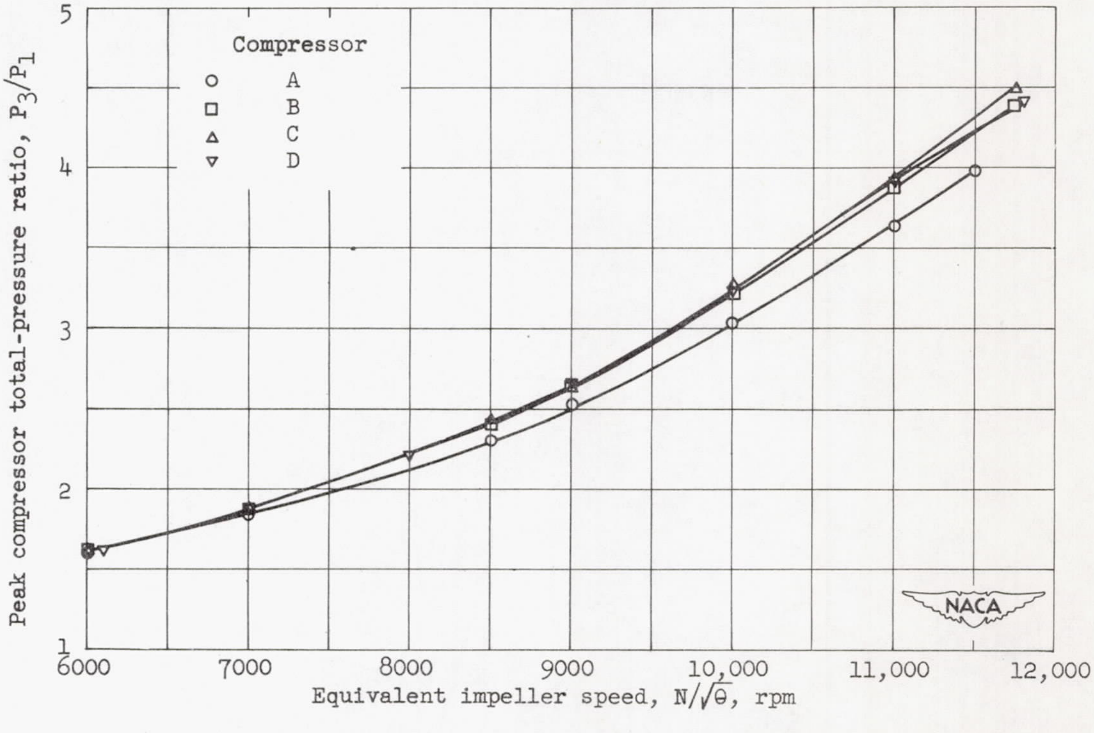

Figure 16. - Variation of peak compressor pressure ratio with speed for four compressors.